Desalination and Water Treatment
www.deswater.com

doi: 10.5004/dwt.2022.28260

253 (2022) 24–38
March

Manufacture and characterization of flat microfiltration membrane based on Moroccan pyrophyllite clay for pretreatment of raw seawater for desalination

Abdellah Talidi[a], Abdelmjid Bouazizi[b,c,d,*], Ahlam Essate[d], Abdelaali Karim[d], Abdellah Aaddane[d], Mohamed Ouammou[d], Rachid Saadani[a], Saad Alami Younssi[d]

[a]*Laboratory for the Study of Advanced Materials and Applications, Faculty of Sciences of Meknes, Higher School of Technology of Meknes, Moulay Ismail University of Meknes, Morocco, emails: talidi@gmail.com (A. Talidi), rachidsaadani@gmail.com (R. Saadani)*
[b]*Department of Sciences, Ecole Normal Superieure, Moulay Ismail University of Meknes, 50000 Morocco, email: abdelmjidbouazizi@gmail.com/abdelmjid.bouazizi-etu@etu.univh2c.ma (A. Bouazizi)*
[c]*Laboratory of Materials, Membranes and Nanotechnology, Faculty of Sciences, Moulay Ismail University, PB 11201, Zitoune, Meknes, Morocco*
[d]*Laboratory of Materials, Membranes and Environment, Faculty of Sciences and Technologies of Mohammedia, Hassan II University of Casablanca, Morocco, emails: ahlam.essate@gmail.com (A. Essate), karimabdelaali@gmail.com (A. Karim), aaddanea@yahoo.fr (A. Aaddane), mouammou@yahoo.fr (M. Ouammou), alamiyounssisaad@yahoo.fr (S.A. Younssi)*

Received 29 September 2021; Accepted 25 January 2022

ABSTRACT

The work explores the preparation and characterization of flat pyrophyllite membrane for microfiltration. The pyrophyllite clay was characterized by X-ray fluorescence, X-ray diffraction and thermogravimetric-differential thermal analysis to determine both its chemical and mineralogical composition also to understand its thermal behavior with respecting the sintering temperature. The ceramic membrane was made under uniaxial pressing of pyrophyllite clay and starch followed by sintering at different temperatures. The optimal temperature of 1,150°C presents a flat membrane with a porosity of 40.50%, an average pore size of 0.80 μm, a mechanical strength of 30 MPa and a permeability of 1,000 L h^{-1} m^{-2} bar^{-1}. Besides, the membrane exhibited good turbidity removal efficiency 99.40% of raw seawater and reduced 77.41% of chemical oxygen demand. Furthermore, the cleaning of the prepared membrane made it possible to recover 80% of its initial water permeability.

Keywords: Pyrophyllite clay; Ceramic membrane; Microfiltration; Seawater pretreatment

1. Introduction

The presence of water in our surroundings is a very precious thing. As we know, the sources of water are very limited to fill the humans needs especially in countries with limited water resources. Indeed, many parts of the world do not have access to drinking water and urgently need economical, reliable and efficient methods to treat local raw water sources [1].

Therefore, great efforts have been devoted to the development of strategies for water treatment. Currently, desalination technology is a promising alternative for the production of potable water from saline and brackish water in regions with arid climates, and it is still seen as the best option to increase water supply in the coming years [2].

The membrane technology is one of the important technologies of seawater treatment currently developed, which is considered a promising approach due to its potential

* Corresponding author.

application in a wide range of industrial processes, its versatility, ease to use, cost-effectiveness and energy-efficiency [3]. Thus, they have undergone significant developments for many applications for pretreatment of seawater for desalination in terms of microfiltration (MF) and ultrafiltration (UF) and they are considered as the most critical membrane technologies.

Nowadays, polymer membranes are widely available and they have been used extensively for the pretreatment of seawater due to their simple functionality and high porosity. However, certain limitations such as easy dirt build-up and short life make these membranes impractical for the long term. Indeed, these limitations have stimulated more efforts towards developing more durable membranes, such as ceramic membranes that can endure harsh conditions and can last longer [4].

Recently, ceramic membranes have attracted much attention from the scientific community due to their low fouling tendency, better thermal, chemical and mechanical stability and great structural integrity. Also, ceramic membranes are less susceptible to irreversible fouling than polymeric membranes [5]. Besides, they can be adaptable to much more aggressive approaches of cleaning without harmful the membrane integrity [6]. Which allows them to be characterized by a long lifespan (>15 y) and recyclability of the membrane material [7]. Consequently, ceramic membranes can be used for industrial applications which weren't possible before.

Particularly, ceramic membranes of MF are an interesting alternative to explore seawater pretreatment application. These membranes have been used for the separation of solid–liquid in various fields (e.g., chemical, pharmaceutical, food, etc.) as well as for water treatment industry [8]. Presently, the ceramic membranes were used for the pretreatment process for the desalination pilot plant in China. The pretreatment with membranes was flexibly combined with other pretreatment processes and operated at a broad range of environmental conditions [9]. The notable interest in using inorganic membrane especially for MF is because of its many advantages, such as flexibility in configuration and the membrane material which allow achieving the highest recovery of a specific element or compound [6], low thermal expansion and conductivity, excellent thermal shock resistance and chemical and mechanical stability [1]. It's well-known that available commercial ceramic membranes are limited by their high cost which is due to the use of various expensive oxides such as alumina, titania, zirconia and silica, also to the fact that these oxides often require high sintering temperature that increases energy consumption [10,11]. Therefore, the use of natural materials is the best solution to reduce the price of ceramic membranes [12]. For several years great effort has been devoted to the preparation of MF ceramic membranes using different low-cost materials such as phosphate, perlite, pozzolan, clay, etc. In the same perspective, Misrar et al. [13] elaborated a ceramic membrane of MF made from Moroccan Ghassoul clay and they studied the addition effect of the calcareous algae on the microstructural properties of this membrane. Singh et al. [14] developed a new low-cost tubular ceramic membrane-based kaolin for recovery of lignin from water and methanol. Li et al. [15] investigated an alumina-mullite composite-based hollow fiber ceramic membrane by phase-inversion and sintering method Indian bentonite clay and zeolite were successfully exploited to prepare a ceramic membrane in order to remove copper from the aqueous [16]. In addition, natural phosphate was used in the membrane technology field whether for the fabrication of natural zeolite clinoptilolite-phosphate composite membranes for water desalination by pervaporation [17]. Recently, in our laboratory some ceramic membranes of MF were successfully prepared from Moroccan geomaterials. Achiou et al. [19], studied the preparation and characterization of tubular membrane based on pozzolan for pretreatment of seawater [18]. A membrane made from natural bentonite clay used for wastewater textile treatment and clarification of tanning effluent was prepared by Bouazizi et al. [12]. Saja et al. [3] fabricated a membrane from perlite for the treatment of textile effluent. Also, phosphate and natural clay were exploited for manufacturing flat membranes by uniaxial pressing method, these membranes were used for seawater pretreatment [20,21]. Newly, Mouratib et al. [22] have manufactured a low-cost membrane based on alumina and silica-rich water treatment sludge, this flat membrane was used for wastewater filtration.

In general, much effort has been dedicated to the synthesis of alternative nature-based membranes using clay. Among these clay types and as a mineral substance, pyrophyllite is a cheap and abundant naturally-occurring clay. Also, it is a crystalline hydrated aluminosilicate with a chemical composition of $Al_2O_3{\cdot}4SiO_2H_2O$, which is composed of two tetrahedral layers surrounded by one octahedral layer interconnected by oxygen ions [23]. Pyrophyllite clay has recognized the most significant attention owing to its physical and chemical properties, which it provides high refractory and average plasticity properties to the ceramic and it exhibits hydrophilic behavior extremely desired to water filtration. In fact, pyrophyllite clay has been a growing interest in many domains such as catalysis [24], adsorption [23] and in preparation of ceramic membranes. Much research on the development of pyrophyllite membranes has been reported in the literature. Jeong et al. [25] successfully developed a pyrophyllite-alumina ceramic membrane for domestic wastewater treatment. Low-cost pyrophyllite-based tubular membrane was prepared and applied in submerged fluidized bed membrane reactor added with granular activated carbon as fluidized particles for synthetic dye removal [26]. Ha et al. [27] fabricated an alumina-coated pyrophyllite-diatomite composite support and reported an initial decrease in the average pore size of a pyrophyllite-diatomite composite support layer from 1.02 to 0.12 μm by depositing an alumina coating layer. Furthermore, the elaboration of pyrophyllite membrane by dry route could lead to obtaining membrane with new performances. Uniaxial pressing is the most suitable technique for flat membrane manufacturing because of its simplified and fast shaping process in comparison with other usual techniques of preparation such as extrusion [3].

According to this point of view, this study aims to prepare and characterize inorganic membrane from pyrophyllite clay as a less expensive natural material by a pressing and sintering technique. In order to evaluate and optimize

the membrane properties, five sintering temperatures from 1,000°C to 1,200°C were investigated and the resulting membranes were characterized in terms of porosity, mechanical strength, pore sizes and water permeability. The performance of the optimized flat pyrophyllite membrane was evaluated for pretreatment of raw seawater to use it as feed for reverse osmosis. Finally, the study of fouling phenomena of the pyrophyllite membrane was carried.

2. Materials and methods

2.1. Raw materials

Pyrophyllite is a dioctahedral 2:1 clay mineral without interlayer cations (similar to talc). It is white, micaceous and feels greasy. The natural Moroccan pyrophyllite extracted from Gunfouda Region (located in the south of Morocco) was employed as principal raw materials for porous ceramic synthesis. Its color appears as white to yellowish-white. The pyrophyllite sample was crushed into small fragments, grounded into a fine powder and sieved through a 63 μm sieve. Corn starch (RG03408, Cerestar) was used as a porosity agent. Sodium hydroxide (NaOH, 98 wt.%) was acquired from Solvachim.

2.2. Ceramic membrane preparation

Firstly, after grinding, pyrophyllite clay was dried at 100°C for 4 h then sieved using a sieve of 63 μm. 90 wt.% of the obtained clay powder and 10 wt.% of starch were mixed and homogenized in mortar. The homogeneous mixture was poured into a cylindrical mold then subjected to uniaxial pressure at 954 bar using a hydraulic press during 10 min. The obtained green disk with a diameter of 4 cm and a thickness of 2 mm was sintered at several temperatures in a programmable furnace (Nabertherm L9/13/P320) according to a thermal program and taking into account the results of thermal analysis in agreement with the differential thermal analysis (DTA)/thermogravimetric analysis (TGA) results. The temperature was increased from room temperature to the first plateau at 250°C for 2 h to remove absorbed and constitutional water then to a second plateau at 480°C for organic matter decomposition. Finally, the temperature was raised to the last plateau for sintering at a temperature ranging from 1,000°C to 1,200°C. After sintering the flat membrane was naturally cooled down to room temperature. All flat disks were sintered at a holding temperature and ramp of 2 h and 5°C/min respectively.

2.3. Experiments of filtration

Filtration experiments were performed out on tangential MF using stainless steel with a filtration area of 5.30 cm^2. Fig. 1 illustrates the laboratory pilot used in this study. This pilot consists of a circulation pump, feed tank of 4 L, membrane housing and pressure gauges. The hydraulic permeability of optimized membrane was determined by distilled water filtration under various pressures at room temperature. According to Darcy's law, the permeability L_p (L h^{-1} m^{-2} bar^{-1}) is considered as a permeate flow function J_w (L h^{-1} m^{-2}) and the corresponding applied transmembrane pressure (ΔP) that varied from 0 to 4 bar. The flux and permeability were calculated by Eqs. (1) and (2), respectively. It should be noted that each filtration experiment was carried out on three different membrane samples.

$$J_w = \frac{V}{A \times t} \tag{1}$$

$$J_w = L_p \times \Delta P \tag{2}$$

where V (L) is the volume of permeate, A (m^2) is the effective membrane area and t (h) is the filtration time.

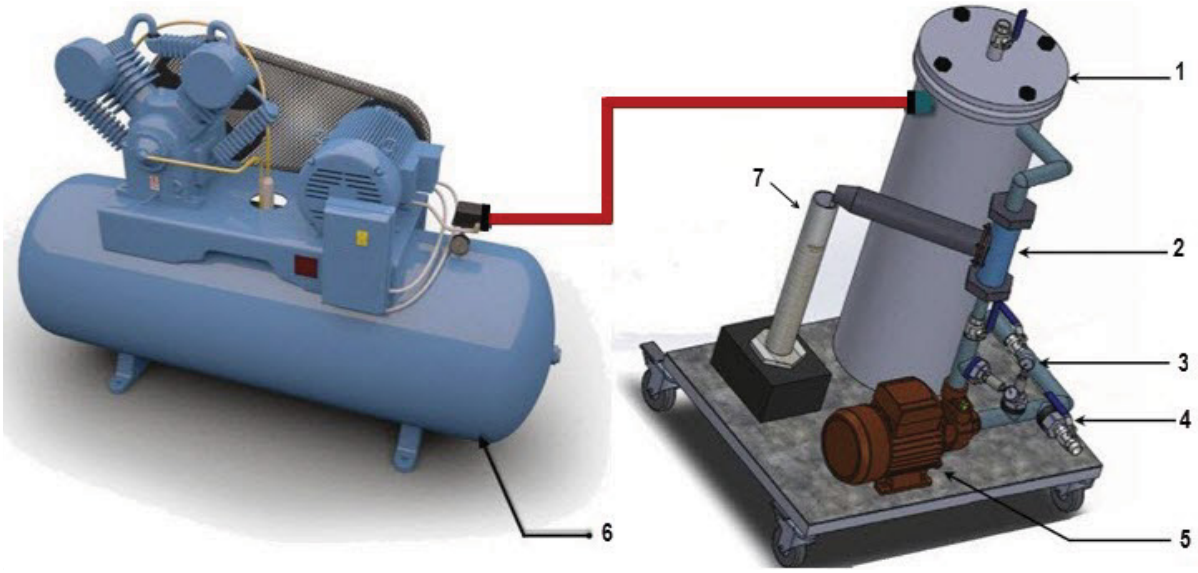

Fig. 1. Lab-scale pilot used in this study. 1: Feed tank, 2: Membrane housing, 3: Valve, 4: Pressure gauge, 5: Circulation pump, 6: Compressor, 7: Permeate.

The performance of elaborated membrane was evaluated by the pretreatment of raw seawater under a pressure of 1 bar for 2 h. This raw seawater was collected from the Atlantic Ocean near Mohammedia City in Morocco. To remove the larger particles each sample was filtered firstly through a sieve of 50 μm. Additionally, the membrane was soaked in bi-distilled water for 24 h before any filtration test. The main analyzed parameters to judge the performance of the MF membrane were flux, pH, conductivity, turbidity, absorbance and chemical oxygen demand (COD). The rejection ratio R(%) was calculated according to the following formulas Eq. (3).

$$R(\%) = \frac{X_{\text{feed}} - X_{\text{permeate}}}{X_{\text{feed}}} \times 100 \tag{3}$$

where X_{feed} and X_{permeate} are the values of turbidity, absorbance or COD in the feed and permeate respectively.

To study the fouling phenomena in detail, four empirical models including complete pore blocking [Eq. (4)], standard pore blocking [Eq. (5)], intermediate pore blocking [Eq. (6)] and cake filtration [Eq. (7)] were used respectively to describe flux decline of the pyrophyllite membrane during the MF experiments of the two feed solutions.

$$\ln\left(J_w^{-1}\right) = \ln\left(J_0^{-1}\right) + K_t \tag{4}$$

$$J_w^{-0.5} = J_0^{-0.5} + K_t \tag{5}$$

$$J_w^{-1} = J_0^{-1} + K_t \tag{6}$$

$$J_w^{-2} = J_0^{-2} + K_t \tag{7}$$

where J_w is the flux, t is the filtration time, K is the slope and J_0 is the y-intercept.

In order to describe the flux recovery capacity of the MF membrane used for raw seawater pretreatment, antifouling characteristics of pyrophyllite membrane were investigated at room temperature under a pressure of 1 bar. Firstly, the fouled pyrophyllite membrane was rinsed with distilled water then 0.1 M NaOH solution using the conventional cross-passage method for 1 h. Secondly, four antifouling parameters are determined: flux recovery ratio (FRR), total flux decline ratio (TFR), reversible flux decline ratio (RFR) and irreversible flux decline ratio (IFR) defined respectively by Eqs. (8)–(11) as reported by Shokri et al. [28]:

$$\text{FRR} = \frac{J_{w1}}{J_{w0}} \times 100 \tag{8}$$

$$\text{TFR} = \frac{J_{w0} - J_{\text{wp}}}{J_{w0}} \times 100 \tag{9}$$

$$\text{RFR} = \frac{J_{w1} - J_{\text{wp}}}{J_{w0}} \times 100 \tag{10}$$

$$\text{IFR} = \frac{J_{w0} - J_{w1}}{J_{w0}} \times 100 \tag{11}$$

where J_{w0} is the water permeate flux, J_{wp} is the permeate flux of raw seawater, J_{w1} is the water permeate flux of cleaned membrane during 1 h.

2.4. Characterization techniques and analyses

Firstly, the particle-size distribution of pyrophyllite powder was performed using laser diffraction particle size analyzer (Mastersizer 2000, Malvern). The X-ray fluorescence analysis was carried on Spectro Xepos (AMETEK). The X-ray diffraction (XRD) was recorded with the use of PANalytical X'Pert Pro X-ray diffractometer using CuKα radiation source (λ = 1.5406 Å). The crystalline phases were identified by the JCPDS (Joint Committee on Powder Diffraction Standards) database. The thermal analyses (TGA/DTA) were performed using a thermobalance of VersaTherm type under air and αAl_2O_3 as reference with a heating rate of 5°C/min.

The porosity and water absorption of the prepared membrane were determined by the Archimedes method measured according to the international standards ASTM C373-88. The microscopic analysis was performed using scanning electron microscopy (SEM) operating at 10 kV (Quattro S, FEG FEI) to study the morphology and texture of membrane surface. The pore-size distribution of the membrane was estimated by image processing of SEM's pictures using ImageJ software (Version 1.44e) [2]. The SEM micrographs are randomly chosen. From the selected sections, the pore-size distributions representing the existing porous texture of the membrane were evaluated. A large number of pores (over 250) were examined in order to determine the distribution. The average pore size (μm) is calculated using the following Eq. (12).

$$d = \sqrt{\frac{\sum_{i=1}^{n} n_i \cdot d_i^2}{\sum_{i=1}^{n} n_i}} \tag{12}$$

where n_i is the number of pores and d_i is the pore diameter.

These results were validated by their comparison with hydraulic pore diameter using the extended Hagen–Poiseuille equation according to Eq. (13) [29].

$$d = 2\sqrt{\left(\frac{L_p 8\mu\tau l}{\varepsilon}\right)} \tag{13}$$

where d is the pore diameter (m), L_p is the permeability (m sPa^{-1}), μ is the water viscosity (0.00089 Pa s), τ is the tortuosity factor (generally taken as 1), l is the thickness of the membrane (m) and ε is the porosity of the membrane (%).

Three-point bending test evaluated the mechanical resistance of each sintered membrane according to the ASTM C674-88 standard [30]. The load displacement curves of indirect tensile and flexural strength were acquired at a loading rate of 0.1 mm min^{-1} utilizing a 1 kN Shimadzu Screw Flat Grips. The dimensions of rectangular specimens were 2 mm × 20 mm × 60 mm respectively.

Physical and chemical parameters of raw seawater and permeate were examined and characterized using several

techniques. The conductivity and pH were measured using a Consort C561 pH-meter. The turbidity was measured using a HACH 2100Q Turbidimeter. The COD was measured by oxidation in acidic medium by the excess of potassium dichromate, oxidizable materials under the conditions of the test in the presence of silver sulfate as catalyst and mercury sulfate according to method used by Mouiya et al. [30].

3. Results and discussion

3.1. Pyrophyllite clay characterization

3.1.1. Particle size analysis

The particle-size distribution of pyrophyllite powder after sieving raw material in a 63 μm sieve is shown in Fig. 2. It is clearly observed that the particle-size distribution is fairly narrow. Furthermore, the distribution of the grains consists essentially of a single homogeneous majority fraction. Overall, 90% of the particles have a diameter less than 40.10 μm. The average diameter is approximately d_{50} = 7.50 μm.

3.1.2. Chemical analysis

The pyrophyllite is a hydrous aluminum silicate with $Si_4Al_2O_{10}(OH)_2$ as standard composition [31]. The chemical composition of the pyrophyllite quantified in the form of oxides is reported in Table 1. It can be noted that, the natural clay is essentially formed of a large amount of 65.40 wt.% of SiO_2, 22.10 wt.% of Al_2O_3 and K_2O and Fe_2O_3 in lower proportion. The SiO_2/Al_2O_3 mass ratio is of the order of 3 which shows that pyrophyllite is an aluminosilicate. Additionally, low amounts of sodium and magnesium oxides are present in the form of impurities. Therefore, the chemical analysis indicated that this pyrophyllite sample contained 95% of pure pyrophyllite [32].

3.1.3. Micrograph and microchemical analysis

Fig. 3 shows the SEM view of the pyrophyllite powder (≤63 μm). The clay micrograph shows a granular structure, aggregates are randomly distributed and material grains of different sizes. Energy-dispersive X-ray spectroscopy (EDX) was carried out to identify the elements present in the natural material studied. The results obtained are in agreement with the chemical analyzes. It follows that silica and alumina are the essential constituents of natural pyrophyllite.

3.1.4. Mineralogical analysis

The recorded XRD analysis of the pyrophyllite sample is given in Fig. 4. The phase identification with the aid of the JCPDS X-ray powder data file showed that the crystalline phases of the natural clay were mainly pyrophyllite as a monoclinic double-layer pyrophyllite, diaspore and quartz [33,34]. It can be noted that, the reaction between pyrophyllite and diaspore at high temperature has an effect on the increase of mechanical strength as was reported previously in the literature [31].

3.1.5. Thermal analysis

TGA and DTA results of pyrophyllite clay are shown in Fig. 5. It can be observed that, there are three mass losses

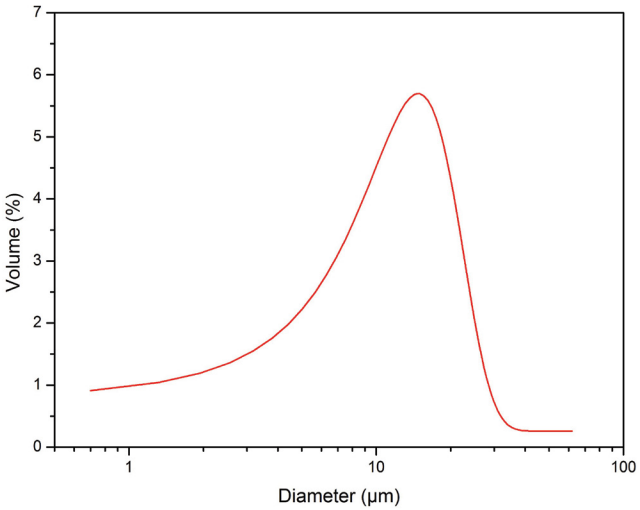

Fig. 2. Particle-size distribution of pyrophyllite powder.

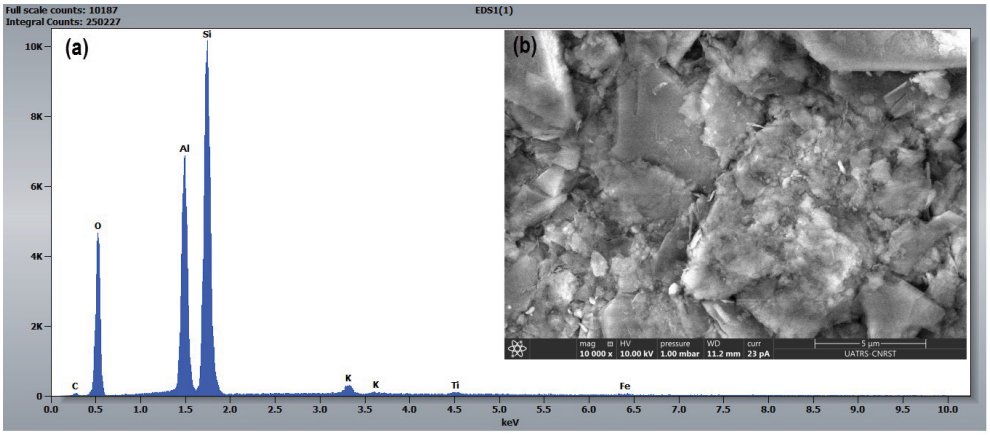

Fig. 3. Analysis of the pyrophyllite clay: (a) EDX analysis and (b) SEM image.

Table 1
Chemical composition of pyrophyllite clay

Oxides	wt.%
SiO_2	65.40
Al_2O_3	22.10
Fe_2O_3	3.12
CaO	1.58
Na_2O	0.15
K_2O	4.40
TiO_2	0.14
MgO	0.30
LOT[a]	3.20

[a]Loss on ignition at 1,000°C.

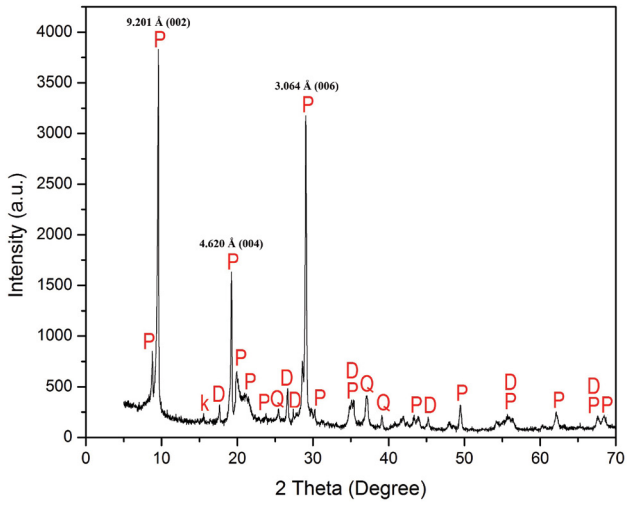

Fig. 4. XRD pattern of the pyrophyllite powder.

during the heating of the pyrophyllite sample. The weight loss of 0.37 wt.% observed between 50°C and 250°C is due to the departure of free and adsorbed water. It corresponds to endothermic phenomenon [35]. The second mass loss of 2.37 wt.% that appears in the TGA curve between 445°C and 755°C is attributed to the removal of octahedral hydroxyl from diaspore and pyrophyllite [36]. That also results in the two endothermic peaks centered at 508°C and 580°C on the DTA curve respectively [33]. A second dehydroxylation of pyrophyllite causes the other mass loss of 0.36 wt.% over a wide temperature range of 755°C to 920°C in the TGA curve, accompanying a slight endothermic peak centered at about 760°C in the DTA curve.

3.2. Characterization of pyrophyllite membrane

3.2.1. Porosity and water absorption

Fig. 6 presents the variations of porosity and water absorption of pyrophyllite membrane as a function of the sintering temperature ranging from 1,000°C to 1,200°C. As can be seen, clear and apparent changes were observed in the porosity and water absorption as the sintering temperature was increased. The both parameters continuously decline with sintering temperature from 45.00% to 18.00% for porosity and from 22.50% to 10.50% for water absorption. This high values of porosity and water absorption obtained at 1,000°C could be explained by the high weight loss (about 12.80 wt.%) during thermal treatment [20]. In the temperature range from 1,050°C to 1,150°C, a small evolution is observed for the porosity with also a maximum at 1,150°C (40.5%) but more presented as a plateau in the middle temperature range (porosity changes scarcely around 0.5%). While water absorption decrease from 22% at 1,050°C to 20.10% at 1,150°C before it decreases sharply to 10.50% at 1,200°C. This is due in particular to the increase of shrinkage of sintered membranes. Consequently, a significant increase of apparent density

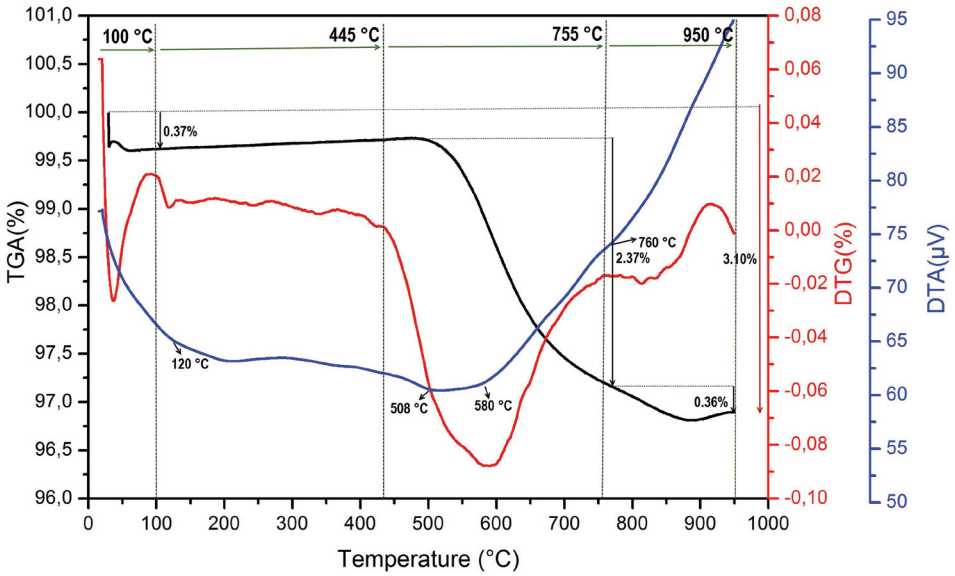

Fig. 5. DTA, TGA and differential thermogravimetric analysis curves of pyrophyllite clay.

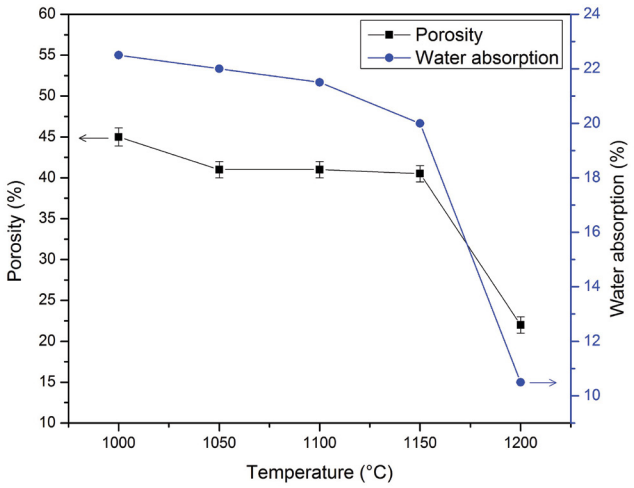

Fig. 6. Evolution of porosity and water absorption vs. sintering temperature.

and then a diminution of water absorption was observed. Differently, the both characteristics decrease with sintering temperature from 1,150°C to 1,200°C. In the case of porosity, it significantly drops from 40.50% to 18.10%. This then allows the reduction of membrane macrovoids which are attributed to smaller pores in the densified membrane structures [2]. This behavior is compatible with the less porous aspects of SEM pictures in Fig. 7. In addition, the presence of alkali oxides as Na_2O, K_2O and MgO in pyrophyllite material also contributes to the formation of vitreous phase at 1,200°C, which leads subsequently to creating dense ceramic [37].

3.2.3. SEM characterization

To provide further evidence in support of the Archimedes test results, the top surface micrograph of pyrophyllite membranes sintered at various temperatures was observed using SEM to evaluate their microstructure (Fig. 7). It is clearly seen from SEM images that sintering temperature significantly affects the morphology of membrane and two important observations that can be drawn. Firstly, the pore size of the pyrophyllite membrane diminished with the increase of sintering temperature. Secondly, increasing of the sintering temperature led to the melting of material particles, thus reducing the porosity of the membrane [38]. At 1,000°C, the membrane is poorly sintered, the intergrain pores between grains are relatively large and particles are not well consolidated. The same observations remain valid in the case of 1,050°C. The membranes are poorly sintered and pyrophyllite particles are not well consolidated with each other to ensure a strong ceramic body. Increasing of sintering temperature up to 1,100°C shows that the sintering process has begun, grains partially merge, but it is not yet enough to achieve strong cohesion between pyrophyllite particles [37]. Therefore, this morphology is not likely enough to ensure a strong ceramic body. Thus, the mechanical strength of the pyrophyllite membrane could improve [29]. Notably, a further increase in temperature to 1,150°C leads to intergranular contact between particles. It is clear that the number of pores decreased due to the coalescence of small pores. Therefore, the membrane is characterized by dense morphology and significant closure of pores. It also presents appropriate porous structure with pore size in the microfiltration range. Whereof, it is supposed that the pyrophyllite membrane sintered at 1,150°C exhibits the highest mechanical strength. This agreed with most studies previously reported in the literature on ceramic membranes [12,22]. At highest temperature (1,200°C) the phenomenon of fusion starts and pyrophyllite particles are more closely packed which causes closure of small intergranular pores [39]. Consequently, an important decrease in the porous volume is observed. Usually, this microstructure enhances the mechanical strength of the membrane but negatively affects the porosity. From these SEM observations, it can be noted that 1,150°C is an appropriate sintering temperature to prepare a better membrane from pyrophyllite clay. In any event, any decision about optimal temperature conditions will be done after the determination of the influence of temperature on mechanical strength.

3.2.4. Pore size analysis

The pore-size distribution seen on the surface of ceramic membranes sintered at different temperatures shows a unimodal distribution of the pore diameter (Fig. 8a). It is noted that the evident difference in pore-size distribution between the ceramic membranes is due to the sintering temperature. It can also be observed from this figure that more than 98% of pores have a diameter <2.60 μm for all membranes. For the membrane sintered at 1,000°C, the pore-size distribution consisting of a peak at approximately 1.55 μm and a smaller peak detected at 1.33 μm is believed to represent the sponge-like pores. After increasing the sintering temperature to 1,050°C and 1,100°C, the large peak shifted to 1.22 and 1.00 μm respectively. The pore-size distribution of flat membrane sintered at 1,150°C shows a large peak at 0.75 μm and a smaller peak detected at 1.20 μm, indicating that the pores (circular or oval forms pores) became smaller and the ceramic had a distinct porous structure. It is interesting as well to note that no significant peak was presented at a sintering temperature of 1,200°C, indicating that the ceramic was completely melted, where the pore size of the pyrophyllite membrane decreased due to the pristine pores densification [40].

The variation of the average pore size of the prepared membrane depending on sintering temperatures (Fig. 8b) shows that, the average pore diameter decreases from 1.57 to 0.30 μm in the range of 1,000°C–1,200°C. This maximum value of pore size observed at 1,000°C is expected according to the pore stability theory and could be attributed both to the elimination of carbonates, which are generally responsible for the generation of large pores, and to the coalescence phenomenon start that occurs between pyrophyllite particles under sintering leading to the formation of large pores with a diameter of around 1.30 μm at 1,050°C [21,41]. However, The average pore size of the membrane sintered at 1,150°C is 0.75 μm. Subsequently, the average pore size continues to decrease to 0.30 μm when the sintering temperature increases 1,200°C. This drop in pore size is due to

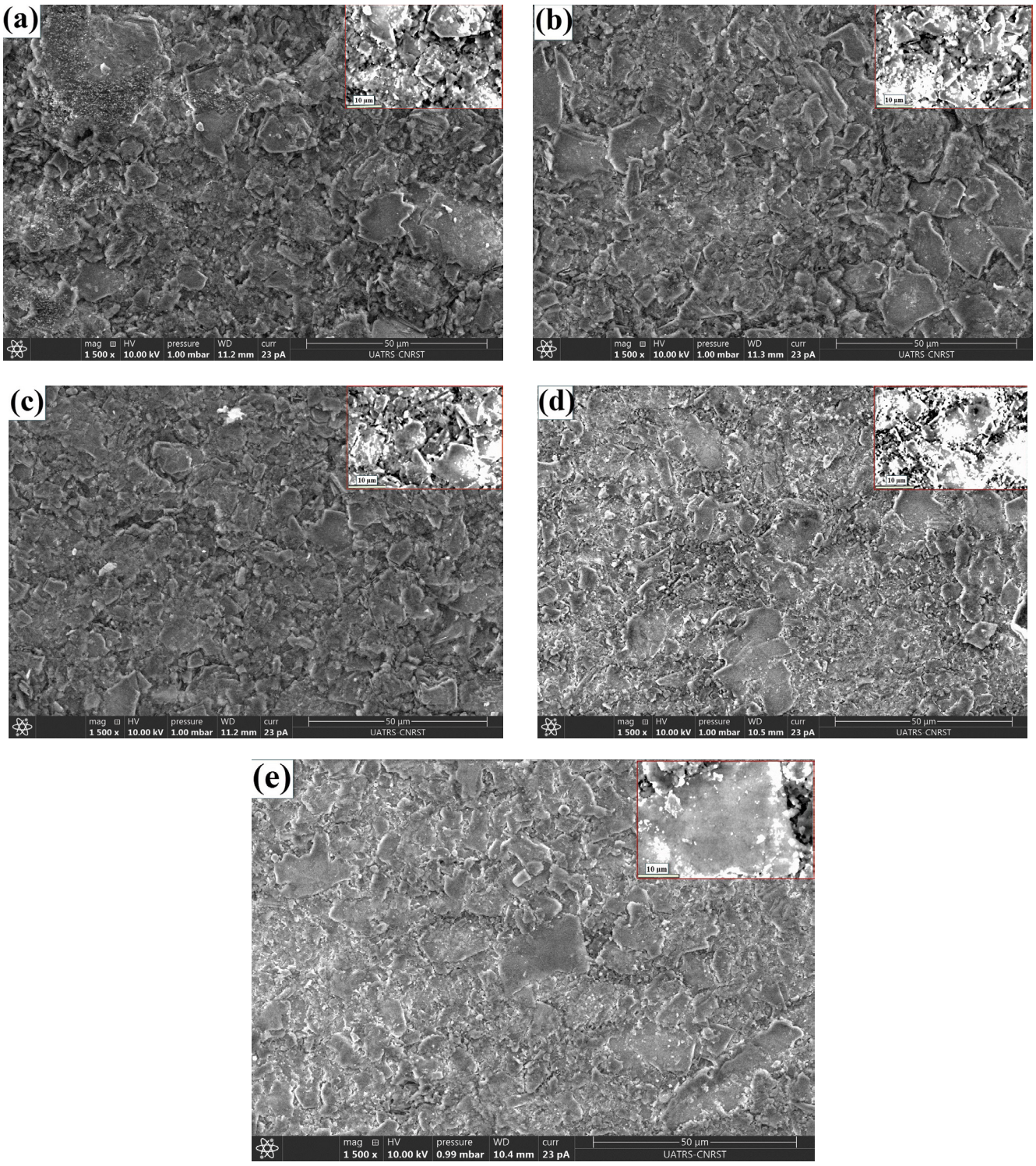

Fig. 7. SEM images of pyrophyllite membrane sintered at different temperature: (a) 1,000°C, (b) 1,050°C, (c) 1,100°C, (d) 1,150°C and (e) 1,200°C.

the partial melting of grain, that resulting by decreasing of inter grain space between grains. Based on these pore size analysis results, it can be seen, that the average pore diameter of pyrophyllite membrane is very small in comparison with other results in the literature [3,12]. All that, keeping an important flexural strength and a high porosity to guarantee a negligible resistance to the flow compared to that of a MF membrane characterized by pore diameters of the order of 0.75 ± 0.05 µm. To observe the difference between the average membrane pore sizes calculated from this method

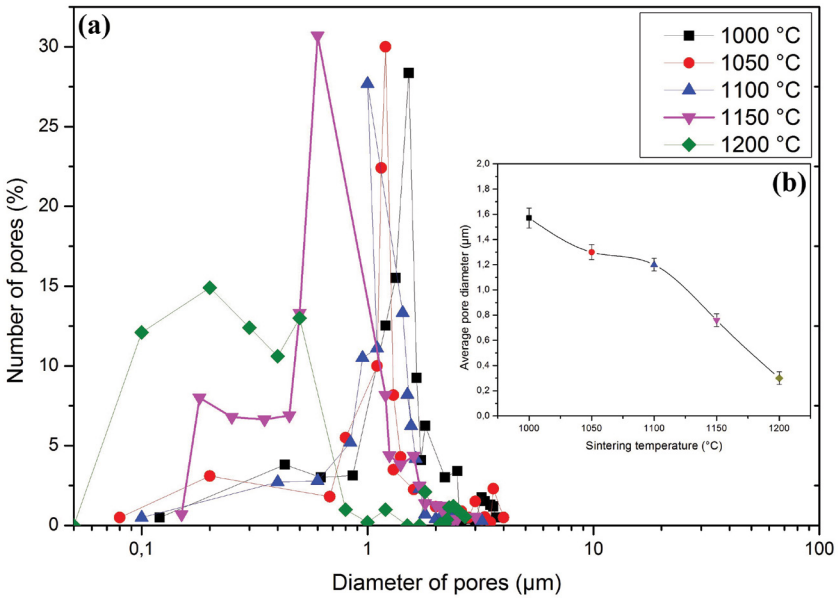

Fig. 8. (a) Pore-size distribution and (b): average pore size of the membranes sintered at various temperatures.

and liquid permeation method, a comparative study is presented at the end of section 3.2.6.

3.2.5. Mechanical resistance

To evaluate the prepared membrane ability to resist of hydraulic pressure during filtration, the flexural strength method is used to measure mechanical resistance. Although, there is a need for a high mechanical strength membrane, denser membranes with fewer voids normally produce lower flows. That's why, the 10 wt.% starch content used as a porosity agent has been added for the study on the effect of sintering temperature on the membrane property [20]. Fig. 9 plots the evolution of membrane mechanical strength with sintering temperature from 1,000°C to 1,200°C. As clearly shown in this figure, the mechanical strength of the pyrophyllite membrane increases from 12.66 to 33 MPa when the sintering temperature rises from 1,000°C to 1,200°C. Normally, this increase is attributed to sintering degree, conducting subsequently to strong cohesion of pyrophyllite particles (caused by partial melting of grains). Especially at higher temperature of 1200°C, the densification of material leads a more consolidated ceramic substance [42]. It should be noted that, this finding is supported by SEM observations and reported by many authors in the literature [21,22,29]. Many studies have been performed to determine the effect of ceramic loading on the ceramic membrane properties. Hubadillah et al. [43] studied the effect of temperature (in range 1,000°C–1,200°C) on the characteristics of kaolin ceramic support prepared by uniaxial pressing technique. This study showed that the mechanical strength has increased significantly from 12.20 to 93.20 MPa by increasing the sintering temperature. The authors reported that the increases in the mechanical properties were attributed to the diminishing of macro voids in the membrane structure. Similar observations have been obtained in our current study, where the macro

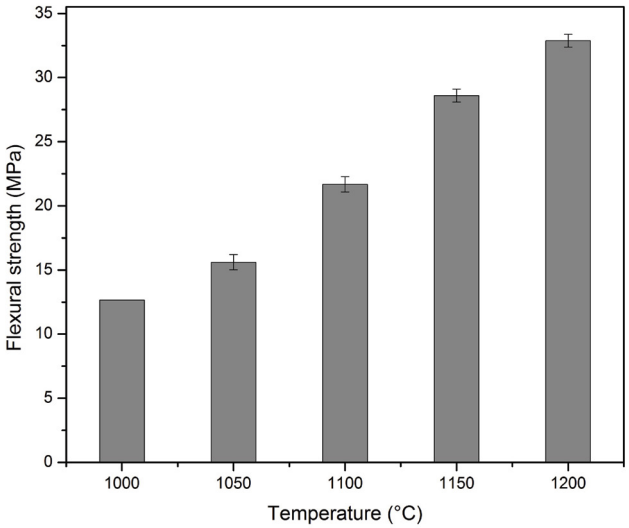

Fig. 9. Variation of mechanical strength of pyrophyllite membrane with sintering temperature.

voids were no longer observed and especially when the sintering temperature has increased to 1,150°C (Fig. 9). In general, sintering temperature strongly affects the mechanical strength of the ceramic membranes and encourage phase transformation and densification [29]. Therefore, this value of 28.60 ± 0.66 MPa at 1,150°C is considered appropriate for the MF experiment and for developing this membrane as a support for an UF membrane.

3.2.6. Water permeability and pore size evaluation

Hydraulic permeability is an extremely important and crucial parameter for defining the operating conditions of the membrane. This parameter was determined using the

variation of the water flux measured after 40 min of filtration (stabilization time of fluxes) with the transmembrane pressure [19]. The typical results of permeability determination of the membranes are presented in Fig. 10. Following Darcy's law, it can be seen that flux is linear for all membranes sintered at different temperatures. The sintering temperature effect on the average membrane permeability is also displayed in Fig. 10a. Firstly, it can be seen that permeability rises from 208 to 1050.50 L h^{-1} m^{-2} bar^{-1} when the temperature increases from 1,000°C to 1,100°C. Thereafter, by increasing the sintering temperature to 1,200°C, the permeability dramatically decreases to reach the minimum value of 510 L h^{-1} m^{-2} bar^{-1}. Presumably, this decrease in permeability could be mainly related to the drop of pore size due to the domination of the densification phenomenon (as shown in 3.2.3) [44]. Whereby, the majority of pores are no longer continuous cross the membrane. These interpretations are consistent with SEM observation of the pyrophyllite membranes. It can also be noted that the main value of the water permeability of 1,000 L h^{-1} m^{-2} bar^{-1} of the sintered pyrophyllite membrane at 1,150°C is a typical value for microfiltration but which remains relatively higher than that found by a membrane produced from commercial alumina [45].

The hydraulic pore diameter of the pyrophyllite membrane was calculated from liquid permeation data of water filtration according to Eq. (6). Fig. 10b shows the hydraulic pore size of the MF membrane as a function of sintering temperature. According to the results of the average membrane pore sizes measured using ImageJ (as commented in the previous paragraph), it can be observed that hydraulic pore size decreases from 0.92 μm at 1,100°C to a minimum value of 0.82 μm at 1,200°C. The average hydraulic pore size of the membrane sintered at 1,150°C is 0.90 ± 0.02 μm. Based on these results, it seems that there is a strong correlation between the porosity, water permeability and pore size. In that sense, Several similar behaviors were pointed out in the literature [21,22]. Therefore, it could be concluded that the pore size estimated from the

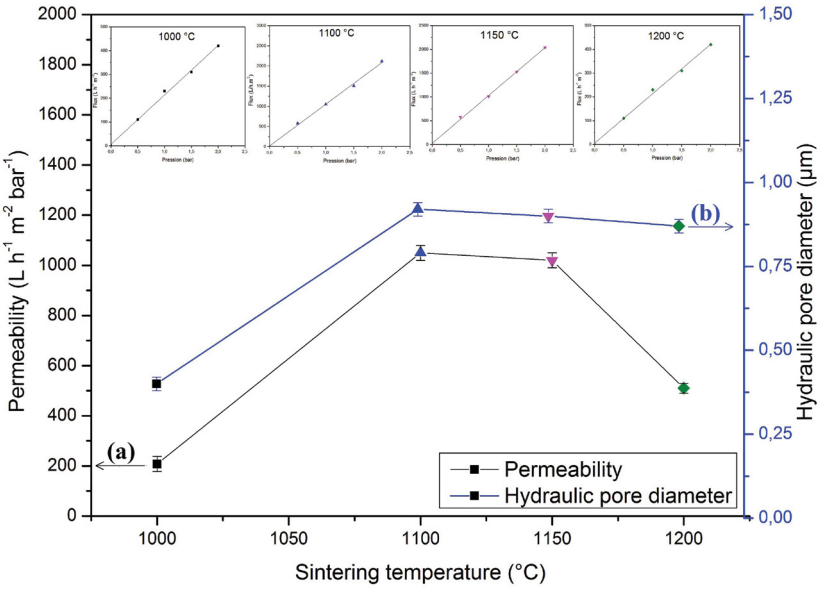

Fig. 10. (a) Permeability and (b) hydraulic pore diameter variation as a function of sintering temperature for membrane prepared membranes.

Table 2
Comparison between the flat pyrophyllite membrane and other ceramic MF membranes in the literature

Material	Membrane configuration	Sintering temperature (°C)	Porosity (%)	Average pore size (μm)	Flexural strength (MPa)	Water permeability (L h^{-1} m^{-2} bar^{-1})	Reference
Perlite (Pressing)	Flat	950	52.11	1.70	21.68	1,433	[3]
Water treatment sludge/clay (Pressing)	Flat	1,050	46.70	0.92	14.5	724	[22]
Phosphate/pozzolan (Pressing)	Flat	1,050	32.7	1.33	15.69	1,732	[29]
Pozzolan (Extrusion)	Tubular	950	41.20	0.37	15.36	1,444	[19]
Clay and banana peel	Flat	1,100 (Support)	40.3	5.5–0.45	19	1,150–550	[30]
Kaolin (Inversion)	Hollow fibre	1,300	58	1.5	15	320	[14]
Pyrophyllite	Flat	1,150	40.50	0.80	30	1,000	This work

water permeation data can be considered more accurate than that estimated from the SEM image analysis. Finally, a compromise between increasing mechanical strength and decreasing porosities of the membranes as sintering temperature increases and based on the excellent characteristics such as SEM analysis, average pore diameter, is reasonable to choose the temperature of 1,150°C as optimal sintering condition. It should be noted that the optimized membrane sintered at this temperature was used for chemical resistance and the filtration experiment.

3.2.7. Potential of pyrophyllite membrane vs other ceramic membranes

Table 2 reports the characteristics of optimized pyrophyllite membrane in comparison with similar MF membranes prepared by other researchers in the literature. According to the results, the pyrophylite membrane owns a high mechanical strength, which is better compared to other membranes with different configurations. Also, the smaller pore size of the pyrophyllite membrane was found to be about 0.75 μm that is closer to that of the commercial membrane. Additionally, results of water permeability indicate that this elaborate membrane is well placed in the low MF range [46]. Furthermore, taking into account cheaper raw material, Table 3 summarizes the price and required sintering temperature of the porophyllite and other common ceramic materials, for example, alumina, zirconia, titania, kaolin and mullite. As shown in this table, the cheaper material and lower sintering temperature have eventually reduced the cost of production of this studied membrane as compared to other commercial ceramic membranes. Consequently, the pyrophyllite membrane is a more desirable alternative in terms of configuration and performance, which will be used ahead for the filtration experiment.

3.3. Microfiltration test

3.3.1. Permeate flux

The variations of permeate fluxes of raw seawater over time are shown in Fig. 11. As it can be observed, the flux decreases with time. This flux decline was assigned to the accumulation of suspended solids, organic, inorganic colloidal and biological matter on the outside and the inside the membrane surface. In addition, it appears that there is a fast fouling phenomenon (caused by pores plugging) in the first 60 min while the slow fouling is observed for the rest of filtration time that increases by the use of tangential filtration. On the other hand, the permeate flux of water is always higher than raw seawater. This is due to the physical properties and nature of each filtered seawater. In point of fact, the more the feed seawater is charged with suspended matter the more the permeate flux decreases.

3.3.2. Pyrophyllite membrane performance

For evaluate the performance in seawater pretreatment. The physicochemical parameters of seawater permeate were measured and presented in Table 4. As indicated in the table, the turbidity decrease from 20 to 0.12 NTU after 120 min of filtration, resulting in a removal percentage of 99.40%. Therefore, the prepared MF membrane with the small average pore size of 0.80 μm allows complete elimination of colloidal particles due to suspended solids and microorganisms present in raw seawater which are responsible for turbidity. Furthermore, the results show

Table 3
Price and required sintering temperature comparison between bentonite clay and other common ceramic materials

Material	Price per kg ($)	Required sintering temperature (°C)	Reference
Alumina	250	1,500–1,700	[27]
Zirconia	78	1,400	[47]
Titania	25	1,400	[48]
Kaolin	~15	1,300–1,500	[49]
Mullite	~15	1,400–1,500	[42]
Pyrophyllite	0.08	1,150	Study

Table 4.
Feed solutions separation performance by pyrophyllite membrane.

Parameter	Raw seawater	Permeate
pH	7.47	8.02
Turbidity (NTU)	20	0.12
COD (mg L^{-1})	6.20	1.41
Conductivity (mS cm^{-1})	50	42.50
Suspended matter (g L^{-1})	1.27	–

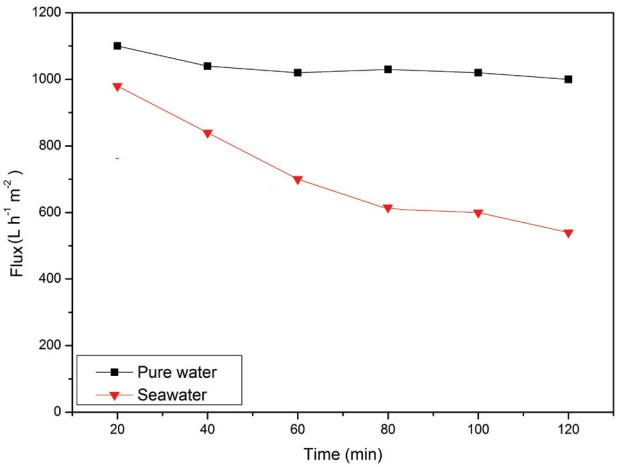

Fig. 11. Time-dependent permeate flux variations of raw seawater for the MF membrane.

that the pyrophyllite membrane can reject 77.41% of COD for 120 min of filtration. Therefore, the great rejections of COD indicate that membrane prepared by pyrophyllite material is effective to retain a big part of organic matter presented in raw seawater. For all the experiments of MF, the results obtained show that the pH values remain almost constant throughout the filtration. As well as, the effect of the MF membrane on the conductivity of the studied raw seawater (50.00 to 42.50 mS cm^{-1}) is unimportant since the MF process is not effective in removing soluble salts in raw seawater.

3.3.3. Fouling phenomena

Fig. 11 depicts the flow of seawater as a function of time, both flows drop off sharply during the first 60 min due to pore blockage. To represent the flux decline of the membrane during the experiments of MF, Fig. 12 shows the linearized graphs of the pore blocking models for the raw seawater. It should be mentioned that the model that well describes the fouling mechanism during filtration of feed solutions is the one with the highest R^2 value [29]. From the results of R^2, it can be inferred that, the MF experiment could involve both cake filtration and intermediate pore blocking models (R^2 of 0.97 and 0.96 respectively) to properly describe flux decline. Suggesting that, seawater contains particles smaller than or equal to the pores of the membrane [22]. In this case, these particles do not necessarily block the total surface of the filter (they can overlap). And/or there are particles larger than the pore size that form a cake on the surface of the pyrophyllite membrane,

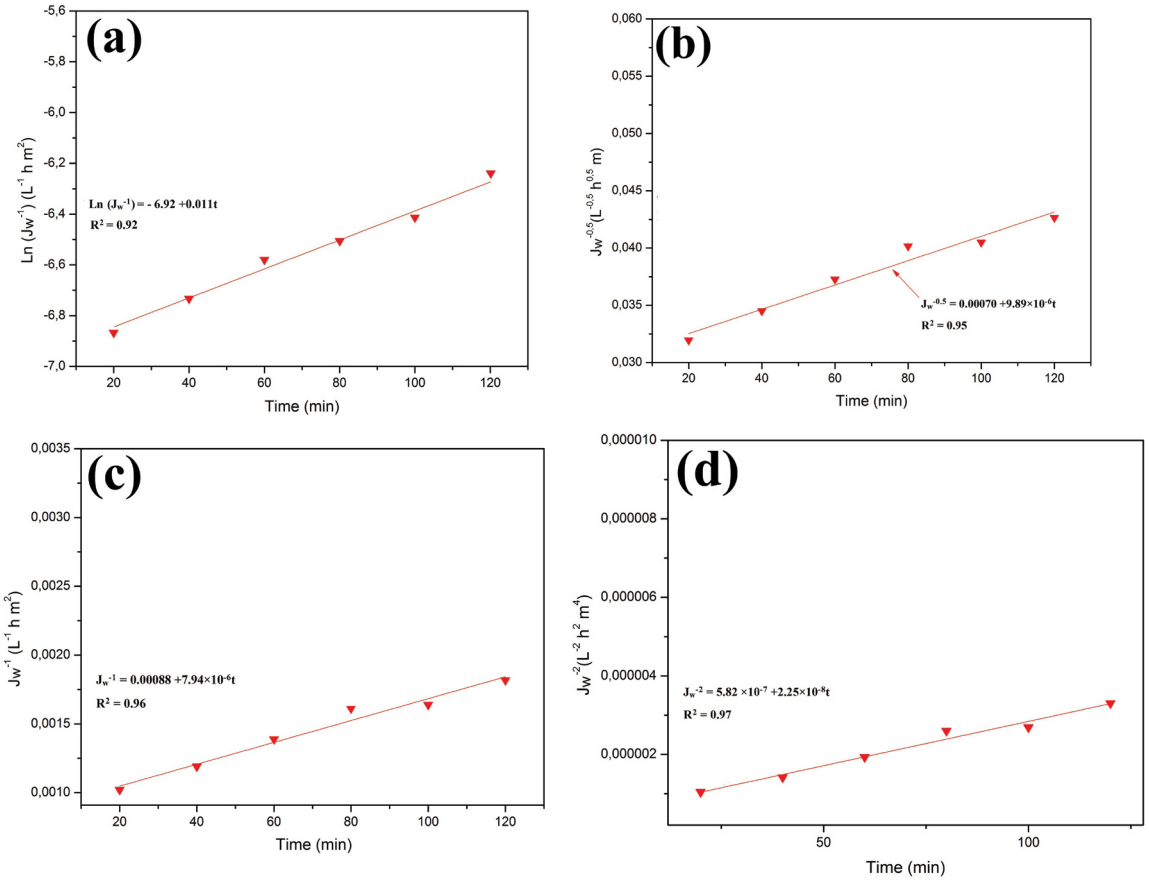

Fig. 12. Linearized graphs of raw seawater: (a) complete pore blocking, (b) standard pore blocking, (c) intermediate pore blocking and (d) cake filtration.

as reported by Beqqour et al. [29]. Furthermore, this typical mechanism mainly contributes to the external fouling of the membrane. Thus, to use the pyrophyllite membrane multiple times, the antifouling study was conducted in more detail to completely understand this phenomenon.

3.3.4. Antifouling study

Four parameters such as FRR, TFR, RFR and IFR related to the fouling study are calculated and summarized in Fig. 13. The value 79.40% of FER indicates that the pyrophyllite membrane used for the filtration of raw seawater recover about 80% of its permeability after cleaning with NaOH solution. This means that the prepared microfiltration membrane has a good antifouling behavior. While, the result of 35.30% found for the TFR parameter explains the percentage of the internal blockage of pores as well as the cake layer formation by the accumulation of particles in suspension on the membrane surface [21]. Regarding the formation of a cake layer that causes the external fouling is evaluated by the RFR parameter calculation. This parameter indicates the presence of 14.70% of external fouling. Therefore, the membrane flux would be easily recovered by the fouled membrane washing using distilled water. However, the IFR value of 20.60% expresses the percentage fouling associated with pore blockage of the membrane. In addition, indicating that backwashing with water and NaOH solution is required. Noting that, this irreversible observed fouling could be explained by the adsorption of certain molecules of tannery effluent dye on the walls of the pores, then partially blocking the transfer of permeate (as indicated previously in Section 3.3.2 – Pyrophyllite membrane performance).

4. Conclusion

A flat porous MF membrane was prepared from natural pyrophyllite by uniaxial pressing method. The chemical analysis shows that siliceous and aluminous material are the most important components of pyrophyllite clay. The sintering temperature significantly affects the filtration properties and microstructure of prepared membranes. The temperature increase remarkably improves porosity, mechanical strength and permeability of membrane up to 1,150°C. SEM analysis confirmed that this membrane is free of cracks and defects. This optimal MF membrane is considered to be the best one, according to the optimized parameters, a porosity of 40.50%, an average pore size of 0.80 μm, a permeability of 1,000 L h^{-1} m^{-2} bar^{-1} and a good mechanical resistance of 30 MP. Indeed, the pyrophyllite membrane demonstrated a notably good performance in seawater pretreatment for desalination. Approximately the totality of turbidity was removed (99.40%). In addition to that, the treatment by the membrane could achieve 77.41% of COD rejection. Finally, the obtained findings suggest that the low-cost pyrophyllite based on membrane could be a perfectly interesting alternative to the traditional methods for pretreatment of seawater for desalination. For future development, as an objective of our further work based on the current work, our laboratory is conducting research to use these pyrophyllite membranes as a support to develop layers suitable for the UF and NF range.

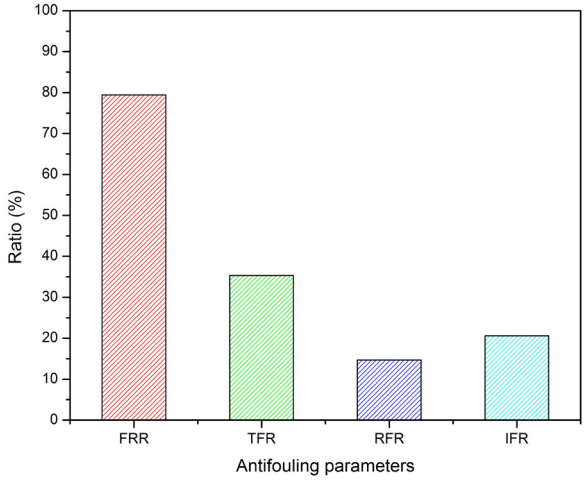

Fig. 13. Fouling parameters of the prepared pyrophyllite membrane.

References

[1] A. Bouazizi, M. Breida, B. Achiou, M. Ouammou, J.I. Calvo, A. Aaddane, S.A. Younssi, Removal of dyes by a new nano–TiO_2 ultrafiltration membrane deposited on low-cost support prepared from natural Moroccan bentonite, Appl. Clay Sci., 149 (2017) 127–135.
[2] A. Bouazizi, M. Breida, A. Karim, B. Achiou, M. Ouammou, J.I. Calvo, A. Aaddane, K. Khiat, S.A. Younssi, Development of a new TiO_2 ultrafiltration membrane on flat ceramic support made from natural bentonite and micronized phosphate and applied for dye removal, Ceram. Int., 43 (2017) 1479–1487.
[3] S. Saja, A. Bouazizi, B. Achiou, M. Ouammou, A. Albizane, J. Bennazha, S.A. Younssi, Elaboration and characterization of low-cost ceramic membrane made from natural Moroccan perlite for treatment of industrial wastewater, J. Environ. Chem. Eng., 6 (2018) 451–458.
[4] S.A. Alftessi, Mohd. H.D. Othman, Mohd. R. Adam, T.M. Farag, A.F. Ismail, M.A. Rahman, J. Jaafar, Md. A. Habib, Y.O. Raji, S.K. Hubadillah, Novel silica sand hollow fibre ceramic membrane for oily wastewater treatment, J. Environ. Chem. Eng., 9 (2021) 104975, doi: 10.1016/j.jece.2020.104975.
[5] F.C. Kramer, R. Shang, L.C. Rietveld, S.J.G. Heijman, Fouling control in ceramic nanofiltration membranes during municipal sewage treatment, Sep. Purif. Technol., 237 (2020) 116373, doi: 10.1016/j.seppur.2019.116373.
[6] S. Saja, A. Bouazizi, B. Achiou, H. Ouaddari, A. Karim, M. Ouammou, A. Aaddane, J. Bennazha, S. Alami Younssi, Fabrication of low-cost ceramic ultrafiltration membrane made from bentonite clay and its application for soluble dyes removal, J. Eur. Ceram. Soc., 40 (2020) 2453–2462.
[7] M. Issaoui, L. Limousy, Low-cost ceramic membranes: synthesis, classifications, and applications, C.R. Chim., 22 (2019) 175–187.
[8] P.S. Goh, A.F. Ismail, A review on inorganic membranes for desalination and wastewater treatment, Desalination, 434 (2018) 60–80.
[9] S.H. Park, Y.G. Park, J.-L. Lim, S. Kim, Evaluation of ceramic membrane applications for water treatment plants with a life cycle cost analysis, Desal. Water Treat., 54 (2015) 973–979.
[10] A. Akbari, M. Omidkhah, Silica-zirconia membrane supported on modified alumina for hydrogen production in steam methane reforming unit, Int. J. Hydrogen Energy, 44 (2019) 16698–16706.
[11] R. Liu, A.K.Y. Raman, I. Shaik, C. Aichele, S.-J. Kim, Inorganic microfiltration membranes incorporated with hydrophilic silica nanoparticles for oil-in-water emulsion separation, J. Water Process Eng., 26 (2018) 124–130.

[12] A. Bouazizi, S. Saja, B. Achiou, M. Ouammou, J.I. Calvo, A. Aaddane, S. Alami Younssi, Elaboration and characterization of a new flat ceramic MF membrane made from natural Moroccan bentonite. Application to treatment of industrial wastewater, Appl. Clay Sci., 132–133 (2016) 33–40.
[13] W. Misrar, M. Loutou, L. Saadi, M. Mansori, O. Cherifi, S. Vilain, M. Waqif, C. Favotto, Effect of the addition of the calcareous algae on the microstructural properties and filtration performances of membranes manufactured from Ghassoul Moroccan clay, Ceram. Int., 46 (2020) 629–640.
[14] P. Singh, N. Arul Manikandan, M. Purnima, K. Pakshirajan, G. Pugazhenthi, Recovery of lignin from water and methanol using low-cost kaolin based tubular ceramic membrane, J. Water Process Eng., 38 (2020) 101615, doi: 10.1016/j.jwpe.2020.101615.
[15] L. Li, M. Chen, Y. Dong, X. Dong, S. Cerneaux, S. Hampshire, J. Cao, L. Zhu, Z. Zhu, J. Liu, A low-cost alumina-mullite composite hollow fiber ceramic membrane fabricated via phase-inversion and sintering method, J. Eur. Ceram. Soc., 36 (2016) 2057–2066.
[16] S. Abd Hamid, M. Shahadat, B. Ballinger, S. Farhan Azha, S. Ismail, S. Wazed Ali, S. Ziauddin Ahammad, Role of clay-based membrane for removal of copper from aqueous solution, J. Saudi Chem. Soc., 24 (2020) 785–798.
[17] W. An, X. Zhou, X. Liu, P.W. Chai, T. Kuznicki, S.M. Kuznicki, Natural zeolite clinoptilolite-phosphate composite membranes for water desalination by pervaporation, J. Membr. Sci., 470 (2014) 431–438.
[18] S. Tang, J. Li, Z. Zhang, B. Ren, X. Zhang, Comparison of long-term ceramic membrane bioreactors without and with *in-situ* ozonation in wastewater treatment: membrane fouling, effluent quality and microbial community, Sci. Total Environ., 652 (2019) 788–799.
[19] B. Achiou, H. Elomari, A. Bouazizi, A. Karim, M. Ouammou, A. Abderrahman Albizane, J. Bennazha, S. Alami Younssi, I.-E. El Amrani El Hassani, Manufacturing of tubular ceramic microfiltration membrane based on natural pozzolan for pretreatment of seawater desalination, Desalination, 419 (2017) 181–187.
[20] M. Mouiya, A. Abourriche, A. Bouazizi, A. Benhammou, Y. El Hafiane, Y. Abouliatim, L. Nibou, M. Mina Oumam, M. Ouammou, A. Smith, H. Hannache, Flat ceramic microfiltration membrane based on natural clay and Moroccan phosphate for desalination and industrial wastewater treatment, Desalination, 427 (2018) 42–50.
[21] A. Belgada, B. Achiou, S. Alami Younssi, F.Z. Charik, M. Ouammou, J.A. Cody, R. Benhida, K. Khaless, Low-cost ceramic microfiltration membrane made from natural phosphate for pretreatment of raw seawater for desalination, J. Eur. Ceram. Soc., 41 (2021) 1613–1621.
[22] R. Mouratib, B. Achiou, M. El Krati, S.A. Younssi, S. Tahiri, Low-cost ceramic membrane made from alumina- and silica-rich water treatment sludge and its application to wastewater filtration, J. Eur. Ceram. Soc., 40 (2020) 5942–5950.
[23] L. Panda, S.S. Rath, D.S. Rao, B.B. Nayak, B. Das, P.K. Misra, Thorough understanding of the kinetics and mechanism of heavy metal adsorption onto a pyrophyllite mine waste based geopolymer, J. Mol. Liq., 263 (2018) 428–441.
[24] A. El Gaidoumi, J.M. Doña-Rodríguez, E. Pulido Melián, O.M. González-Díaz, J.A. Navío, B. El Bali, A. Kherbeche, Catalytic efficiency of Cu-supported pyrophyllite in heterogeneous catalytic oxidation of phenol, Arabian J. Sci. Eng., 44 (2019) 6313–6325.
[25] Y. Jeong, S. Lee, S. Hong, C. Park, Preparation, characterization and application of low-cost pyrophyllite-alumina composite ceramic membranes for treating low-strength domestic wastewater, J. Membr. Sci., 536 (2017) 108–115.
[26] R. Ahmad, M. Aslam, E. Park, S. Chang, D. Kwon, J. Kim, Submerged low-cost pyrophyllite ceramic membrane filtration combined with GAC as fluidized particles for industrial wastewater treatment, Chemosphere, 206 (2018) 784–792.
[27] J.-H. Ha, S.Z. Abbas Bukhari, J. Lee, I.-H. Song, C. Park, Preparation processes and characterizations of alumina-coated alumina support layers and alumina-coated natural material-based support layers for microfiltration, Ceram. Int., 42 (2016) 13796–13804.
[28] E. Shokri, E. Shahed, M. Hermani, H. Etemadi, Towards enhanced fouling resistance of PVC ultrafiltration membrane using modified montmorillonite with folic acid, Appl. Clay Sci., 200 (2021) 105906, doi: 10.1016/j.clay.2020.105906.
[29] D. Beqqour, B. Achiou, A. Bouazizi, H. Ouaddari, H. Elomari, M. Ouammou, J. Bennazha, S. Alami Younssi, Enhancement of microfiltration performances of pozzolan membrane by incorporation of micronized phosphate and its application for industrial wastewater treatment, J. Environ. Chem. Eng., 7 (2019) 102981, doi: 10.1016/j.jece.2019.102981.
[30] M. Mouiya, A. Bouazizi, A. Abourriche, A. Benhammou, Y. El Hafiane, M. Ouammou, Y. Abouliatim, S.A. Younssi, A. Smith, H. Hannache, Fabrication and characterization of a ceramic membrane from clay and banana peel powder: application to industrial wastewater treatment, Mater. Chem. Phys., 227 (2019) 291–301.
[31] A. Bentayeb, M. Amouric, J. Olives, A. Dekayir, A. Nadiri, XRD and HRTEM characterization of pyrophyllite from Morocco and its possible applications, Appl. Clay Sci., 22 (2003) 211–221.
[32] Y. Miyah, A. Lahrichi, M. Idrissi, S. Boujraf, H. Taouda, F. Zerrouq, Assessment of adsorption kinetics for removal potential of Crystal Violet dye from aqueous solutions using Moroccan pyrophyllite, J. Assoc. Arab Univ. Basic Appl. Sci., 23 (2017) 20–28.
[33] G. Li, J. Zeng, J. Luo, M. Liu, T. Jiang, G. Qiu, Thermal transformation of pyrophyllite and alkali dissolution behavior of silicon, Appl. Clay Sci., 99 (2014) 282–288.
[34] T.K. Mukhopadhyay, S. Ghatak, H.S. Maiti, Pyrophyllite as raw material for ceramic applications in the perspective of its pyro-chemical properties, Ceram. Int., 36 (2010) 909–916.
[35] A. Terzić, D. Radulović, M. Pezo, J. Stojanović, L. Pezo, Z. Radojević, L. Andrić, Prediction model based on artificial neural network for pyrophyllite mechano-chemical activation as an integral step in production of cement binders, Constr. Build. Mater., 258 (2020) 119721, doi: 10.1016/j.conbuildmat.2020.119721.
[36] J. Zhang, Y. Zhou, M. Jiang, J. Li, J. Sheng, Removal of methylene blue from aqueous solution by adsorption on pyrophyllite, J. Mol. Liq., 209 (2015) 267–271.
[37] R. Sule, I. Sigalas, Effect of temperature on mullite synthesis from attrition-milled pyrophyllite and α-alumina by spark plasma sintering, Appl. Clay Sci., 162 (2018) 288–296.
[38] M. Mouiya, A. Bouazizi, A. Abourriche, Y. El Khessaimi, A. Benhammou, Y. El Hafiane, Y. Taha, M. Oumam, Y. Abouliatim, A. Smith, H. Hannache, Effect of sintering temperature on the microstructure and mechanical behavior of porous ceramics made from clay and banana peel powder, Results Mater., 4 (2019) 100028, doi: 10.1016/j.rinma.2019.100028.
[39] A. Talidi, N. Saffaj, K. El Kacemi, S.A. Younssi, A. Albizane, A. Chakir, Processing and characterization of tubular ceramic support for microfiltration membrane prepared from pyrophyllite clay, Sci. Stud. Res., 12 (2011) 263–268.
[40] J.-H. Ha, J. Lee, I.-H. Song, S.-H. Lee, The effects of diatomite addition on the pore characteristics of a pyrophyllite support layer, Ceram. Int., 41 (2015) 9542–9548.
[41] T. Hondo, Z. Kato, K. Yasuda, F. Wakai, S. Tanaka, Coarse pore evolution in dry-pressed alumina ceramics during sintering, Adv. Powder Technol., 27 (2016) 1006–1012.
[42] M.H. Abd Aziz, M.H.D. Othman, N.A. Hashim, M.R. Adam, A. Mustafa, Fabrication and characterization of mullite ceramic hollow fiber membrane from natural occurring ball clay, Appl. Clay Sci., 177 (2019) 51–62.
[43] S.K. Hubadillah, M.H.D. Othman, T. Matsuura, A.F. Ismail, M.A. Rahman, Z. Harun, J. Jaafar, M. Nomura, Fabrications and applications of low cost ceramic membrane from kaolin: a comprehensive review, Ceram. Int., 44 (2018) 4538–4560.
[44] B. Hatimi, J. Mouldar, A. Loudiki, H. Hafdi, M. Joudi, E.M. Daoudi, H. Nasrellah, I.-T. Lançar, M.A. El Mhammedi, M. Bakasse, Low cost pyrrhotite ash/clay-based inorganic membrane for industrial wastewaters treatment, J. Environ. Chem. Eng., 8 (2020) 103646, doi: 10.1016/j.jece.2019.103646.

[45] Q. Gu, T.C.A. Ng, W. Zang, L. Zhang, Z. Lyu, Z. Zhang, H.Y. Ng, J. Wang, Surface engineered alumina microfiltration membranes based on rationally constructed core-shell particles, J. Eur. Ceram. Soc., 40 (2020) 5951–5958.
[46] R. Makabe, K. Akamatsu, R. Tatsumi, O. Koike, S.-i. Nakao, Numerical simulations of lift force and drag force on a particle in cross-flow microfiltration of colloidal suspensions to understand limiting flux, J. Membr. Sci., 621 (2021) 118998, doi: 10.1016/j.memsci.2020.118998.
[47] S.J. Ahn, A. Takagaki, T. Sugawara, R. Kikuchi, S. Ted Oyama, Permeation properties of silica-zirconia composite membranes supported on porous alumina substrates, J. Membr. Sci., 526 (2017) 409–416.
[48] Y. Dong, S. Hampshire, J. Zhou, B. Lin, Z. Ji, X. Zhang, G. Meng, Recycling of fly ash for preparing porous mullite membrane supports with titania addition, J. Hazard. Mater., 180 (2010) 173–180.
[49] S.K. Hubadillah, M.H.D. Othman, M.A. Rahman, A.F. Ismail, J. Jaafar, Preparation and characterization of inexpensive kaolin hollow fibre membrane (KHFM) prepared using phase inversion/sintering technique for the efficient separation of real oily wastewater, Arabian J. Chem., 13 (2020) 2349–2367.